Prediction of Triple Point Fermions in Simple Half-Heusler Topological Insulators

Hao Yang,[1] Jiabin Yu,[2] Stuart S. P. Parkin,[1] Claudia Felser,[3] Chao-Xing Liu,[2] and Binghai Yan[4,*]
[1]Max Planck Institute of Microstructure Physics, Weinberg 2, 06120 Halle, Germany
[2]Department of Physics, Pennsylvania State University, University Park, Pennsylvania 16802, USA
[3]Max Planck Institute for Chemical Physics of Solids, 01187 Dresden, Germany
[4]Department of Condensed Matter Physics, Weizmann Institute of Science, Rehovot 7610001, Israel
(Received 30 May 2017; published 28 September 2017)

We predict the existence of triple point fermions in the band structure of several half-Heusler topological insulators by *ab initio* calculations and the Kane model. We find that many half-Heusler compounds exhibit multiple triple points along four independent C_3 axes, through which the doubly degenerate conduction bands and the nondegenerate valence band cross each other linearly nearby the Fermi energy. When projected from the bulk to the (111) surface, most of these triple points are located far away from the surface $\bar{\Gamma}$ point, as distinct from previously reported triple point fermion candidates. These isolated triple points give rise to Fermi arcs on the surface, that can be readily detected by photoemission spectroscopy or scanning tunneling spectroscopy.

DOI: 10.1103/PhysRevLett.119.136401

The discovery of topological insulators (TIs) [1,2] has generated much interest in the search for other novel topological states in condensed matter physics and materials science. As quasiparticle analogs of elementary particles of the standard model, Dirac fermions [3–6] and Weyl fermions [7–14] have recently been found in several materials (see reviews Refs. [15,16]). More recently, several exotic types of fermions, which do not have elementary particle counterparts, have been theoretically predicted as quasiparticle excitations near certain band crossing points that are protected by specific space-group symmetries [17,18]. In particular, triple point (TP) fermions have been predicted in many materials with triply degenerate band crossing points [19–25]. These predictions have stimulated intensive experimental studies to search for their signatures, for example, using angle-resolved photoemission spectroscopy (ARPES) [26] and transport properties [27].

TPs can be viewed as an intermediate phase between fourfold degenerate Dirac points and twofold degenerate Weyl points. They also give rise to Fermi arcs when projected onto certain specific crystal facets. However, the detection of TP-induced Fermi arcs remains challenging from the material point of view. A pair of TPs are protected by the C_{3v} symmetry group (generated by a C_3 rotation and a σ_v mirror operation) in certain compounds [19–24], for example, tensile-strained mercury telluride (HgTe) [19], molybdenum phosphide (MoP) [20], and antiferromagnetic (AFM) half-Heusler compounds (e.g., GdPtBi) [24]. Even presuming that samples can be grown, the natural cleavable surface is usually the facet that is perpendicular to the C_{3v} axis. Consequently, two TPs at the unique C_{3v} axis are projected to the same $\bar{\Gamma}$ point of the surface Brillouin zone (BZ), resulting in the disappearance of Fermi arcs, as shown in a recent ARPES measurement on MoP [26]. Therefore, TP materials with easily measurable Fermi arcs are still required for the final experimental verification of TP fermions.

In this work, we predict the existence of multiple TPs in several half-Heusler compounds in which the detection of Fermi arcs by ARPES and other surface sensitive techniques such as scanning tunneling spectroscopy should be straightforward. The face-centered-cubic lattice of half-Heusler compounds has four equivalent C_{3v} axes (e.g., the [111] axis) and, thus, can host four (or multiples of four) pairs of TPs. When projected onto the (111) surface, an easily cleavable plane [28,29], TPs at the [111] axes merge into the surface $\bar{\Gamma}$ point while the other three (or a multiple of three) pairs of TPs appear away from $\bar{\Gamma}$, leading to Fermi arcs that link these individual TPs on the surface. Combining *ab initio* band structure calculations and the $k \cdot p$ Kane model, we predict several TP candidate half-Heusler materials, including, for example, YPtBi, LuPtBi, and GdPtBi (the paramagnetic phase). The TPs and resultant extended Fermi arcs are revealed in our calculations, and await experimental proof.

Ternary half-Heusler compounds have been extensively studied in the search for TIs [28–34] and Weyl semimetals [35–38]. The band structure of Heusler TIs has been identified as being topologically identical to HgTe [39]. For example, the conduction and valence bands touch each other at the Γ point, where the wave functions are comprised mainly of p orbitals and are, therefore, named Γ_8 bands, as shown in Fig. 1(a). The fourfold degeneracy at the Γ point is protected by time-reversal symmetry (TRS) and T_d group symmetry. The s-type Γ_6 bands located below Γ_8, thus give rise to an inverted band structure. Along each C_{3v} axis (e.g., the [111] direction), Γ_8 bands split into one doubly degenerate band (labeled as Λ_6 according to the C_{3v} symmetry) and two nondegenerate bands (labeled as $\Lambda_{4,5}$) due to the absence of inversion symmetry in the T_d group. The Λ_6 bands cross the $\Lambda_{4,5}$ bands since Λ_6 and $\Lambda_{4,5}$ bands disperse oppositely for large k [see Fig. 1(a)]. As already pointed out in Ref. [19], TPs exist at the crossing point

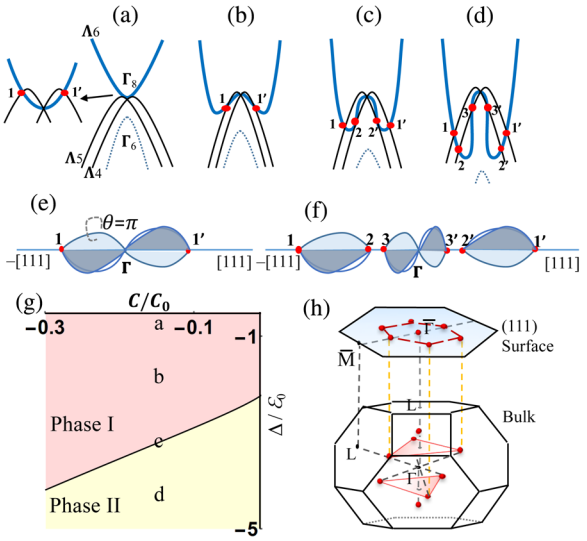

FIG. 1. Evolution of band structures with increasing numbers of triple points (TPs). (a) HgTe-type band structure along the line $L-\Gamma-L$. The Γ_8 bands (solids curves) lie above Γ_6 (dotted curves). The Γ_8 bands split into doubly degenerate Λ_6 (thick solid blue curve) and nondegenerate Λ_4 and Λ_5 bands (thin solid black curves) along the C_3 axis ($\Gamma-L$). Here Λ_6 crosses $\Lambda_{4,5}$, forming TPs (filled red circles) very close to the Γ point, where No. 1 and No. $1'$ represent a TP and its time-reversal partner, respectively. (b) Heusler-type band structure. The Λ_6 bands exhibit a double valley shape, pushing a pair of TPs out from the Γ point. (c), (d) Heusler-type band structure with two and three pairs of TPs along one C_{3v} axis, respectively. (e) Corresponding to the band structures in (a) and (b), three nodal lines (blue curves) inside the C_{3v} mirror planes connect a pair of TPs (1 and $1'$) along the C_3 axis by passing the Γ point. (f) Corresponding to the band structure in (d), the nodal lines connects these three pairs of TPs. (g) Phase diagram of TPs with respect to the band inversion strength Δ/ϵ_0 and the linear splitting term C/C_0 of $\Lambda_{4,5}$. Within the phase diagram, (a)–(d) correspond to the band structures of (a)–(d), respectively. (h) Distribution of TPs in the bulk Brillouin zone and their projection onto the (111) surface. The surface Fermi arcs that connect different TPs are illustrated by red dashed lines.

between Λ_6 and Λ_4 (or Λ_5) bands. Unfortunately, the TPs that are located extremely close to the Γ point (~0.8% of the $\Gamma-L$ distance) [19] cannot be resolved by currently available techniques. In contrast, TPs in some Heusler materials can be pushed to very large momenta, because their Λ_6 bands exhibit a peculiar double-valley feature that is absent in HgTe [e.g., see Fig. 1(b)]. As illustrated in Fig. 1(b), a pair of TPs may exist near the Γ point along the C_3 axis ($\Gamma-L$), where two TPs are related by TRS and protected by C_3 rotational symmetry. Given four C_3 axes, four pairs of TPs form inside the first bulk BZ. When projected onto the (111) surface, three pairs are isolated from each other and are far from the surface $\bar{\Gamma}$ point, giving rise to Fermi arcs connecting these six TPs [Fig. 1(h)].

We first construct a phase diagram to reveal the emergence and properties of TPs in half-Heusler compounds based on the Kane model [40], in order to guide the material search. The crystal symmetry of Half-Heusler materials is described by the space group $F\bar{4}3m$ and the point group T_d [41], respectively, and the corresponding low energy physics can be described by the six-band Kane model with two Γ_6 bands and four Γ_8 bands. Along any of the four C_3 axes, two Γ_6 bands are still degenerate, labeled as Λ_6^- bands, according to the irreducible representations of C_{3v} spin double group, while four Γ_8 bands are split into one doubly degenerate band, denoted as Λ_6^+ bands, and two nondegenerate bands, denoted as Λ_4 and Λ_5 bands, respectively. For the momentum close to Γ along the C_3 axis, the Λ_6^+ bands disperse quadratically while the $\Lambda_{4,5}$ bands disperse linearly with opposite velocities for two branches due to the linear C term in the Kane Hamiltonian. Thus, the Λ_6^+ bands must locate between two $\Lambda_{4,5}$ bands for small momenta. For larger momenta, the Λ_6^+ bands bend up and thus will be always above two $\Lambda_{4,5}$ bands that bend down. Thus, we conclude that at least one pair of TPs due to the crossing between the Λ_6 bands and the upper branch of $\Lambda_{4,5}$ bands must exist. According to energy dispersion along the C_3 axis for the Kane model (see details in Ref. [42]), we find that 1, 2, or 3 pairs of TPs can exist in one C_3 axis, depending on model parameters. The phase diagram as a function of the parameter C, which determines the energy splitting of two $\Lambda_{4,5}$ bands, and the gap Δ between Γ_6 and Γ_8 states, which influence the effective mass of Λ_6^+ bands, is shown in Fig. 1(g). For a small Δ, strong hybridization beween Λ_6^+ and Λ_6^- bands can lead to a positive effective mass for the Λ_6^+ band and thus results in 1 pair of TPs between the Λ_6^+ bands and the upper branch of $\Lambda_{4,5}$ bands [Fig. 1(a)] in phase I in Fig. 1(g). As Δ increases, the effective mass for the Λ_6^+ bands become negative, leading to a double-hump structure [Fig. 1(b)]. With Δ increasing to a critical value, the double-hump Λ_6^+ bands can touch the lower branch of $\Lambda_{4,5}$ bands, giving rise to one more pair of TPs (TP #2 and $2'$) at the critical line in Fig. 1(g). As Δ further increases, the Λ_6^+ bands can cross the lower branch of $\Lambda_{4,5}$ twice, resulting in 3 pairs of TPs in total for the phase I in Fig. 1(g). TPs are connected by nodal lines and for different phases, we find the connections are different. For the phase I, four nodal lines, three in three mirror planes and one along the C_3 axis, connects the TP #1 to its time-reversal partner TP $1'$, passing through the Γ point, as shown in Fig. 1(e). The Berry phase around each of three nodal lines in the mirror plane is accumulated to π and characterizes its topological nature (Type-B TPs introduced in Ref. [20]). Three pairs of TPs exist the phase II, with TPs #1 and #2 ($1'$ and $2'$) connected by nodal lines and TPs #3 and $3'$ connected by nodal lines through Γ, as shown in Fig. 1(f).

In addition, we note that TPs can also exist in the normal zinc-blende-type band structures without a band inversion, since Γ_6 bands commonly have different mass from $\Gamma_{4,5}$. It provides an alternative way to search for TPs in traditional

TABLE I. List of triple point (TP) half Heusler materials. The band inversion strength Δ is in units of eV. The number of TPs (#) is shown in Fig. 1. The distance of a TP to the Γ point (Δ_k) is specified as a percentage of the $\Gamma - L$ length. The energy of a TP is given with respect to the Fermi energy (ϵ) in unit of meV.

Material	#	Δ	Δ_k	ϵ	Material	#	Δ	Δ_k	ϵ
LuPtBi	1	−1.52	32.5%	−131	YPtBi	1	−1.07	17.1%	−38
	2		26.7%	−144		2		14.3%	−27
	3		1.3%	154		3		0.4%	50
LuAuPb	1	−1.07	24.2%	105	GdPtBi	1	−1.02	14.1%	−22
	2		15.9%	142	LuPdBi	1	−0.69	11.9%	−8
	3		5.0%	201	LaPtBi	1	−0.82	1.3%	8

semiconductors, where the Luttinger model [46] is applicable.

To search for ideal material candidates, we have performed *ab initio* band structure calculations for a large number of half-Heusler compounds using density-functional theory (DFT) with the generalized gradient approximation. We have identified many candidate materials exhibiting TPs with a large momentum separation in their band structure, as listed in Table I. For example, TPs #1 and #2 of *R*PtBi (R = Y, Lu), LuAuPb, LuPdBi, and TP #1 of GdPtBi (paramagnetic phase) lie at large momenta greater than %10 of the $\Gamma - L$ length. The TP #3 is located too close to the Γ point for the observation. We also list the band inversion strength between the Γ_6 and Γ_8 bands in Table I to demonstrate the evolution of the band structure. Roughly consistent with the above phase diagram, TPs shift to larger momenta as the band inversion is enhanced. For comparison, we also show the band structure of LaPtBi in Fig. 2, where TPs appear very close to the Γ point. For convenience, we term materials with TPs at large momenta as long-TP materials, and those with TPs at tiny momenta as short-TP materials. When the Fermi energy crosses a TP in GdPtBi and YPtBi, the TP behaves as the touching point between hole and electron pockets, thereby showing the same feature as a type-II Weyl semimetal [47,48]. Many half-Heusler compounds are known to exhibit much larger band inversions than HgTe. Thus, it is not surprising to find long-TP materials here. It has been reported that optimized exchange-correlation functionals in DFT tend to reduce the band inversion of Heusler compounds [49]. We note that this functional correction remains of the general order of the band inversion strength between different Heuslser materials, where long-TP materials can still be found in the large band inversion region.

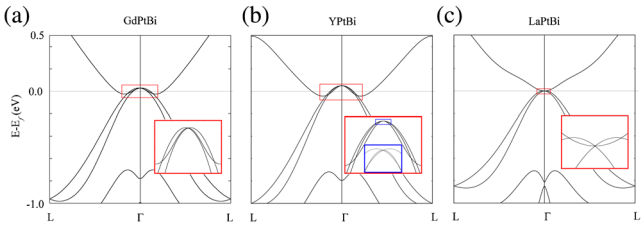

FIG. 2. Bulk band structures with triply degenerate band crossings. The long-TP materials (a) GdPtBi with 2 TPs along the C_3 axis and (b) YPtBi with 6 TPs. The band dispersion along the C_3 axis near the Γ point are magnified to show the TPs on the right panels. (c) The short-TP material LaPtBi are shown for comparison.

The existence of Fermi arcs on the surface is a hallmark of TPs for their experimental detection. When projected to the (111) surface, six TPs (TPs #1 and 1′) locate at the $\bar{\Gamma} - \bar{M}$ line. Because a typical TP is equivalent to two degenerate Weyl points (WPs) with opposite charities, typically two Fermi arcs are expected to emerge from a TP. A natural choice is that these two Fermi arcs end at two neighboring TPs separately (one possible case is that a Fermi arc connects those two WPs and disappear as two WPs merge to be a TP). As a consequence, six Fermi arcs form a hexagonlike Fermi surface. We first employed a tight-binding regularization of the Kane model and calculated the surface states on a half-infinite (111) surface. As shown in the surface band structure of Fig. 3(a) with only 1 TP along the $\bar{M} - \bar{\Gamma}$ line, a surface band disperses from the Brillouin zone boundary to the center. Along $\bar{K} - \bar{\Gamma}$, it runs very close to the $\bar{\Gamma}$ point and merges into the bulk background. From $\bar{M}$ to $\bar{\Gamma}$, however, it ends exactly at the TP. On the Fermi surface at E_F crossing the TP, one can clearly see that six Fermi arcs connect six TPs, forming a hexagon shape. Each Fermi arc starts at a TP and ends at the neighboring TP [Fig. 3(a)-(iii)]. Outside the hexagon of Fermi arcs, there is a larger Fermi ring due to the same surface band. When 3 TPs exist along the $\bar{M} - \bar{\Gamma}$ line [Fig. 3(b)], the original surface band still ends at the TP #1 while a new surface band appears to link TP #2 and TP #3 although it is weak in intensity. On the Fermi surface, one can observe that six Fermi arcs connect six TPs #1 [Fig. 3(b)-(ii)] and also six TPs #2 [Fig. 3(b)-(iii)]. We note that the Fermi arc states penetrate deeply into the bulk, similar to the Fermi arcs of a Weyl semimetal TaAs [50,51], since they appear close to the bulk pocket boundary on the Fermi surface. Therefore, we can summarize two important features of TP surface states. (i) The surface band ends at the TP #1 position in the energy dispersion along $\bar{M} - \bar{\Gamma}$.

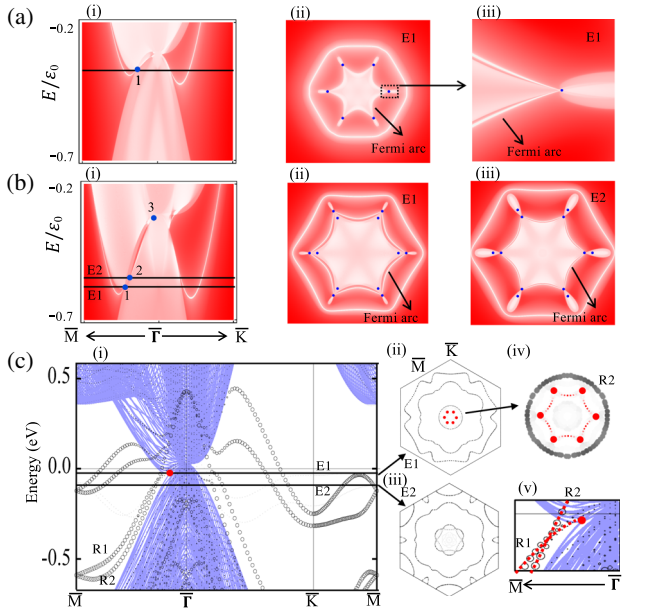

FIG. 3. Surface band structures. (a),(b) Band structure calculated by the tight-binding model on a half-infinite surface with 1 and 3 TPs along $\bar{\Gamma}-\bar{M}$, respectively. Red color stands for low surface intensity and white for strong surface intensity. The triple points are marked by blue points. (c) DFT band structure calculated on a slab model for GdPtBi (paramagnetic phase). (i) The size of the white circles represents the surface contribution and, thus, large circles show the surface states. Bulk bands are indicated by blue curves as a background, where the triple point is shown as the red point. $R1$ and $R2$ are a pair of Rashba-like surface states. (ii) and (iii), Fermi surfaces corresponding to energy $E1$ (crossing the triple point) and $E2$, respectively. The flowerlike Fermi surface in (iii) was measured in previous ARPES experiments. (iv) Magnified inner Fermi ring of (ii). Fermi arcs (red dotted lines) are artificially added as guides to the eye, for they are missing in the DFT band structure due to the finite slab thickness. (v) Expanded view near the triple point. Red dotted lines highlight $R1$ and $R2$ bands. The $R1$ band crosses $R2$ and later ends at the triple point.

(ii) Six Fermi arcs interconnect six TPs related by C_3 and TRS when E_F crosses the TPs.

Regarding materials we have calculated the surface states of GdPtBi based on *ab initio* DFT calculations within a slab model. The slab model includes 54 atomic layers of the (111) surface and the band structure is projected to the top surface that is terminated by Bi atoms. The projected band structure represents the dispersions of surface states [Fig. 3(c)], which agrees well with previous ARPES measurement [28]. There are several trivial surface states due to Bi dangling bonds in the band structure. We point out a pair of Rashba-like surface bands [noted $R1$ and $R2$ in Fig. 3(c)], which disperse up from -0.6 eV at $\bar{M}$ to above E_F at $\bar{\Gamma}$. When approaching the TP, $R1$ does not disperse up together with $R2$, as ordinary Rashba bands do. Instead, $R1$ crosses $R2$ at energy $E2 = -72$ meV and then ends at the TP at $E1 = -22$ meV [Fig. 3(c)-(v)], fulfilling the first feature of Fermi arc states. Here the surface band structure is a result of the strong hybridization between Fermi arc states and dangling bond states. We point out that the same feature that $R1$ ends at the TP can be found for another long-TP material YPtBi and even a short-TP material LaPtBi; see Ref. [42] for more information. For the Fermi surface corresponding to E_2 [Fig. 3(c)-(iii)], there are two rings forming a flowerlike shape caused by the $R1$-$R2$ crossing. For the Fermi surface corresponding to E_1 [Fig. 3(c)-(ii)], there is only one apparent ring due to $R2$. Here six TPs locate inside the $R2$ ring, where Fermi arcs are expected to exist. However, these Fermi arcs are missing in the DFT band structure. This is due to the finite size effect of the slab model simulations. In experiment, corresponding Fermi arcs should appear but possibly with weak intensity, since they penetrate deeply into the bulk. In previous ARPES experiments, a flowerlike Fermi surface similar to Fig. 3(c)-(iii) was observed for LuPtBi, YPtBi, and GdPtBi [28,29], where $R1$ starts crossing $R2$. However, ARPES did not reach the energy window of TPs, because these Heusler samples are usually hole doped. To fully reach the TP region by ARPES, electron-doped samples are needed to shift E_F by $\sim$50 meV with respect to current samples.

In summary, we have predicted the existence of TP fermions in the band structures of several half-Heusler TIs. By *ab initio* calculations and the $k \cdot p$ Kane model, we have identified the existence of multiple TPs at large momenta in the bulk and revealed the existence of Fermi arcs on the surface. The Fermi arcs states end at the TP position in the energy dispersion along $\bar{M}-\bar{\Gamma}$ and connect neighboring TPs at the Fermi surface. To observe TPs and Fermi arcs, currently available samples may need slightly more electron doping for ARPES studies. Alternatively, two-photon photoelectron spectroscopy or scanning tunneling spectroscopy, which can measure empty states, will be ideal for the detection of TP Fermi arcs. The predicted Heusler TP materials are known to exhibit AFM phase (e.g., GdPtBi) [41] and superconductivity (e.g., LuPtBi and YPtBi) [52,53] at low temperatures. They serve as a new platform to investigate the interplay between TPs and magnetism or superconductivity.

We thank Haim Beidenkopf, Nurit Avraham, and Ady Stern for helpful discussions. B. Y. acknowledges the support by the Ruth and Herman Albert Scholars Program for New Scientists and a research grant from the Willner Family Leadership Institute in Weizmann Institute of Science, Israel and by a grant from the German-Israeli Foundation for Scientific Research and Development (GIF Grant No. I-1364-303.7/2016). C.-X. L. acknowledges support from the Office of Naval Research (Grant No. N00014-15-1-2675).

*binghai.yan@weizmann.ac.il

[1] X.-L. Qi and S.-C. Zhang, Rev. Mod. Phys. **83**, 1057 (2011).
[2] M. Z. Hasan and C. L. Kane, Rev. Mod. Phys. **82**, 3045 (2010).
[3] S. M. Young, S. Zaheer, J. C. Y. Teo, C. L. Kane, E. J. Mele, and A. M. Rappe, Phys. Rev. Lett. **108**, 140405 (2012).
[4] Z. Wang, Y. Sun, X.-Q. Chen, C. Franchini, G. Xu, H. Weng, X. Dai, and Z. Fang, Phys. Rev. B **85**, 195320 (2012).
[5] Z. K. Liu, B. Zhou, Y. Zhang, Z. J. Wang, H. M. Weng, D. Prabhakaran, S.-K. Mo, Z. X. Shen, Z. Fang, X. Dai, Z. Hussain, and Y. L. Chen, Science **343**, 864 (2014).
[6] S. Xu, C. Liu, S. K. Kushwaha, R. Sankar, J. W. Krizan, I. Belopolski, M. Neupane, G. Bian, N. Alidoust, T. R. Chang, H. T. Jeng, C. Y. Huang, W. F. Tsai, H. Lin, P. P. Shibayev, F. C. Chou, R. J. Cava, and M. Z. Hasan, Science **347**, 294 (2015).
[7] X. G. Wan, A. M. Turner, A. Vishwanath, and S. Y. Savrasov, Phys. Rev. B **83**, 205101 (2011).
[8] G. E. Volovik, *The Universe in a Helium Droplet* (Clarendon Press, Oxford, England, 2003).
[9] A. A. Burkov, M. D. Hook, and L. Balents, Phys. Rev. B **84**, 235126 (2011).
[10] H. Weng, C. Fang, Z. Fang, B. A. Bernevig, and X. Dai, Phys. Rev. X **5**, 011029 (2015).
[11] S.-M. Huang, S.-Y. Xu, I. Belopolski, C.-C. Lee, G. Chang, B. Wang, N. Alidoust, G. Bian, M. Neupane, C. Zhang, S. Jia, A. Bansil, H. Lin, and M. Z. Hasan, Nat. Commun. **6**, 8373 (2015).
[12] B. Q. Lv, H. M. Weng, B. B. Fu, X. P. Wang, H. Miao, J. Ma, P. Richard, X. C. Huang, L. X. Zhao, G. F. Chen, Z. Fang, X. Dai, T. Qian, and H. Ding, Phys. Rev. X **5**, 031013 (2015).
[13] S.-Y. Xu, I. Belopolski, N. Alidoust, M. Neupane, G. Bian, C. Zhang, R. Sankar, G. Chang, Y. Zhujun, C.-C. Lee, H. Shin-Ming, H. Zheng, J. Ma, D. S. Sanchez, B. Wang, A. Bansil, F. Chou, P. P. Shibayev, H. Lin, S. Jia, and M. Z. Hasan, Science **349**, 613 (2015).
[14] L. X. Yang, Z. K. Liu, Y. Sun, H. Peng, H. F. Yang, T. Zhang, B. Zhou, Y. Zhang, Y. F. Guo, M. Rahn, D. Prabhakaran, Z. Hussain, S. K. Mo, C. Felser, B. Yan, and Y. L. Chen, Nat. Phys. **11**, 728 (2015).
[15] B. Yan and C. Felser, Annu. Rev. Condens. Matter Phys. **8**, 337 (2017).
[16] N. P. Armitage, E. J. Mele, and A. Vishwanath, arXiv: 1705.01111 [Rev. Mod. Phys. (to be published)].
[17] B. J. Wieder, Y. Kim, A. M. Rappe, and C. L. Kane, Phys. Rev. Lett. **116**, 186402 (2016).
[18] B. Bradlyn, J. Cano, Z. Wang, M. G. Vergniory, C. Felser, R. J. Cava, and B. A. Bernevig, Science **353**, aaf5037 (2016).
[19] S. Zaheer, S. M. Young, D. Cellucci, J. C. Y. Teo, C. L. Kane, E. J. Mele, and A. M. Rappe, Phys. Rev. B **87**, 045202 (2013).
[20] Z. Zhu, G. W. Winkler, Q. S. Wu, J. Li, and A. A. Soluyanov, Phys. Rev. X **6**, 031003 (2016).
[21] G. W. Winkler, Q. S. Wu, M. Troyer, P. Krogstrup, and A. A. Soluyanov, Phys. Rev. Lett. **117**, 076403 (2016).
[22] H. Weng, C. Fang, Z. Fang, and X. Dai, Phys. Rev. B **93**, 241202 (2016).
[23] H. Weng, C. Fang, Z. Fang, and X. Dai, Phys. Rev. B **94**, 165201 (2016).
[24] J. Yu, B. Yan, and C.-X. Liu, Phys. Rev. B **95**, 235158 (2017).
[25] I. C. Fulga and A. Stern, Phys. Rev. B **95**, 241116 (2017).
[26] B. Q. Lv, Z. L. Feng, Q. N. Xu, J. Z. Ma, and L. Y. Kong, Nature (London) **546**, 627 (2017).
[27] C. Shekhar, Y. Sun, N. Kumar, M. Nicklas, K. Manna, V. Suess, O. Young, I. Leermakers, T. Foerster, M. Schmidt, L. Muechler, P. Werner, W. Schnelle, U. Zeitler, B. Yan, S. S. P. Parkin, and C. Felser, arXiv:1703.03736.
[28] C. Liu, Y. Lee, T. Kondo, E. D. Mun, M. Caudle, B. N. Harmon, S. L. Bud'ko, P. C. Canfield, and A. Kaminski, Phys. Rev. B **83**, 205133 (2011).
[29] Z. K. Liu, L. X. Yang, S. C. Wu, C. Shekhar, J. Jiang, H. F. Yang, Y. Zhang, S.-K. Mo, Z. Hussain, B. Yan, C. Felser, and Y. L. Chen, Nat. Commun. **7**, 12924 (2016).
[30] S. Chadov, X. L. Qi, J. K. Kübler, G. H. Fecher, C. Felser, and S. C. Zhang, Nat. Mater. **9**, 541 (2010).
[31] H. Lin, L. A. Wray, Y. Xia, S. Xu, S. Jia, R. J. Cava, A. Bansil, and M. Z. Hasan, Nat. Mater. **9**, 546 (2010).
[32] D. Xiao, Y. Yao, W. Feng, J. Wen, W. Zhu, X.-Q. Chen, G. M. Stocks, and Z. Zhang, Phys. Rev. Lett. **105**, 096404 (2010).
[33] B. Yan and A. de Visser, MRS Bull. **39**, 859 (2014).
[34] J. A. Logan, S. J. Patel, S. D. Harrington, C. M. Polley, B. D. Schultz, T. Balasubramanian, A. Janotti, A. Mikkelsen, and C. J. Palmstrøm, Nat. Commun. **7**, 11993 (2016).
[35] M. Hirschberger, S. Kushwaha, Z. Wang, Q. Gibson, S. Liang, C. A. Belvin, B. A. Bernevig, R. J. Cava, and N. P. Ong, Nat. Mater. **15**, 1161 (2016).
[36] C. Shekhar, A. K. Nayak, S. Singh, N. Kumar, S.-C. Wu, Y. Zhang, A. C. Komarek, E. Kampert, Y. Skourski, J. Wosnitza, W. Schnelle, A. McCollam, U. Zeitler, J. Kübler, S. Parkin, B. Yan, and C. Felser, arXiv:1604.01641.
[37] J. Ruan, S.-K. Jian, H. Yao, H. Zhang, S.-C. Zhang, and D. Xing, Nat. Commun. **7**, 11136 (2016).
[38] J. Cano, B. Bradlyn, Z. Wang, M. Hirschberger, N. P. Ong, and B. A. Bernevig, Phys. Rev. B **95**, 161306 (2017).
[39] B. A. Bernevig, T. L. Hughes, and S. C. Zhang, Science **314**, 1757 (2006).
[40] R. Winkler, S. Papadakis, E. De Poortere, and M. Shayegan, *Spin-Orbit Coupling in Two-Dimensional Electron and Hole Systems* (Springer, New York, 2003), Vol. 41.
[41] P. C. Canfield, J. Thompson, W. Beyermann, A. Lacerda, M. Hundley, E. Peterson, Z. Fisk, and H. Ott, J. Appl. Phys. **70**, 5800 (1991).
[42] See Supplemental Material at http://link.aps.org/supplemental/10.1103/PhysRevLett.119.136401, which includes Refs. [43–45], for more details of model Hamiltonians, calculation methods, and results.
[43] M. I. Aroyo, J. M. Perez-Mato, C. Capillas, E. Kroumova, S. Ivantchev, G. Madariaga, A. Kirov, and H. Wondratschek, Zeitschrift für Kristallographie-Crystalline Materials **221**, 15 (2006).
[44] W. Al-Sawai, H. Lin, R. S. Markiewicz, L. A. Wray, Y. Xia, S.-Y. Xu, M. Z. Hasan, and A. Bansil, Phys. Rev. B **82**, 125208 (2010).
[45] G. Burns, *Introduction to Group Theory with Applications: Materials Science and Technology* (Academic Press, New York, 2014).
[46] J. M. Luttinger, Phys. Rev. **102**, 1030 (1956).
[47] A. A. Soluyanov, D. Gresch, Z. Wang, Q. Wu, M. Troyer, X. Dai, and B. A. Bernevig, Nature (London) **527**, 495 (2015).

[48] Y. Sun, S. C. Wu, M. N. Ali, C. Felser, and B. Yan, Phys. Rev. B **92**, 161107(R) (2015).
[49] W. Feng, D. Xiao, Y. Zhang, and Y. Yao, Phys. Rev. B **82**, 235121 (2010).
[50] R. Batabyal, N. Morali, N. Avraham, Y. Sun, M. Schmidt, C. Felser, A. Stern, B. Yan, and H. Beidenkopf, Sci. Adv. **2**, e1600709 (2016).
[51] H. Inoue, A. Gyenis, Z. Wang, J. Li, S. W. Oh, S. Jiang, N. Ni, B. A. Bernevig, and A. Yazdani, Science **351**, 1184 (2016).
[52] N. P. Butch, P. Syers, K. Kirshenbaum, A. P. Hope, and J. Paglione, Phys. Rev. B **84**, 220504 (2011).
[53] F. F. Tafti, T. Fujii, A. Juneau-Fecteau, S. Rene de Cotret, N. Doiron-Leyraud, A. Asamitsu, and L. Taillefer, Phys. Rev. B **87**, 184504 (2013).